USING SADDLE POINTS FOR SUBPIXEL FEATURE DETECTION IN CAMERA CALIBRATION TARGETS

Luca Lucchese

Sanjit K. Mitra

Department of Electrical and Computer Engineering
Oregon State University, Corvallis, Oregon
Phone: (541) 737 2919, Fax: (541) 737 1300
e-mail: luca@ece.ucsb.edu

Department of Electrical and Computer Engineering
University of California, Santa Barbara, California
Phone: (805) 893 8312, Fax (805) 893 3262
e-mail: mitra@ece.ucsb.edu

ABSTRACT

The determination of realiable features with subpixel accuracy is an important requirement of any camera calibration algorithm. This paper offers a simple and computationally attractive method for extracting X-junctions with subpixel precision from images of calibration checkerboards by showing how the saddle points associated with them can be determined without any surface fitting required by standard feature detection algorithms.

1. INTRODUCTION

Many camera calibration algorithms rely on artificial targets, usually consisting of regular patterns; the 3-D locations of salient features of these patterns as well as their 2-D projections on the image plane of the camera focusing the target have to be determined as accurately as possible in order to estimate the intrinsic and extrinsic parameters of the camera [1]. It has been shown that a feature detector with an accuracy of a few hundredths of a pixel leads to almost perfect calibration parameters, provided that the corresponding 3-D locations are determined with sufficient precision too [2].

Subpixel feature detection is an easy task for patterns made up of regular arrays of circles [3], squares [4], and crosses [5]. Also, regular black-and-white checkerboards are widely used for calibration since their X-junctions can be easily detected [6]. The locations of these features are first estimated with standard corner detection algorithms [7] and then refined towards subpixel accuracy by fitting quadratic functions to surface patches around the detected junctions and computing their extremal points; in general, this method allows for accuracies of the order of a few hundredths of a pixel.

In this paper, we show how this refinement step can be greatly simplified and made more accurate by observing the shape of the intensity profile, regarded as a surface, of a checkerboard image around its X-junctions. In fact, the lowpass filtering necessary to remove the additive Gaussian noise commonly degrading the target images makes the surface very smooth and regular and permits a simple detection of the saddle points marking the X-junctions. No quadratic fitting of the surface is thus necessary, which considerably reduces the computation load; at the same time, the refinement algorithm we propose yields slightly more accurate estimates and shows more robustness against noise.

This paper has three sections. Section 2 presents the traditional algorithm for detecting X-junctions in images of checkerboard patterns for camera calibration and our new refinement step; it also compares the performances of the two in six synthetic images corrupted by various amounts of white Gaussian noise. Section 3 contains the conclusions.

2. SUBPIXEL DETECTION OF X-JUNCTIONS

Let $\psi_r(x)$, $x \in \mathbb{R}^2$, be the image of a calibration checkerboard. Figure 1 shows such an image consisting of 13×13 squares of 30×30 pixels; the overall size of this image is 510×510 pixels. In order to simulate a practical camera calibration[1] scenario a second image $\psi_b(x)$ is derived from $\psi_r(x)$ through the projective warping and blurring operations defined by equations[2]

$$\psi_r(x) = \psi_w \left(\frac{Ax + b}{c^T x + 1} \right), \quad \psi_b(x) = \psi_w(x) \circledast h(x),$$

(1)

where $A = \begin{bmatrix} 1.10 & 0.01 \\ -0.01 & 1.20 \end{bmatrix}$, $b = \begin{bmatrix} 0 \\ 20 \end{bmatrix}$, $c = \begin{bmatrix} 0 \\ 0.0004 \end{bmatrix}$,

---

[1]Lens distortion [1] is not modeled for simplicity.
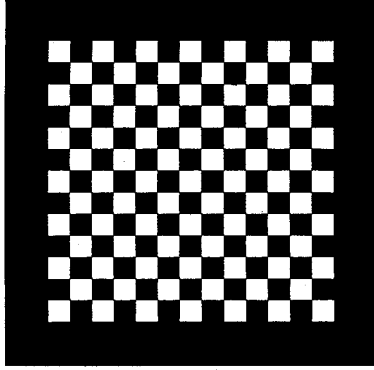[2]The symbol $\circledast$ denotes 2-D linear convolution.

Figure 1: Synthetic image $\psi_r(x)$ of a checkerboard calibration pattern.

SNR (dB)	standard method		our method	
	μ_d	σ_d	μ_d	σ_d
∞	0.0030	0.0015	0.0019	0.0010
33.88	0.0109	0.0057	0.0108	0.0056
27.86	0.0216	0.0112	0.0211	0.0110
21.84	0.0446	0.0233	0.0446	0.0233
15.82	0.0868	0.0453	0.0833	0.0435
12.30	0.1369	0.0715	0.1265	0.0661

Table 1: Mean values μ_d and standard deviations σ_d of the Rayleigh pdf's modeling the error distributions in the examples of Figs. 3 and 4. $SRN = \infty$ indicates that the image is devoid of noise.

and $h(x)$ is a normalized Gaussian filter[3] with aperture $\sigma_h = 1$ [1]; Fig. 3 (a) shows the resulting image $\psi_b(x)$. To mimic real camera calibration situations, five noisy versions $\psi_n(x)$ of $\psi_b(x)$ were obtained by adding zero-mean white Gaussian noise to it with standard deviations $\sigma_n = 0.0125, 0.025, 0.05, 0.1$, and 0.15; these images are displayed in Figs. 3 (d) and (g) and Figs. 4 (a), (d), and (g). The associated signal-to-noise (SNR) ratios, defined as $SNR = 10\log_{10}\left(\int_{\mathbb{R}^2} \psi_b^2(x)\,dx/\sigma_n^2\right)$, are respectively 33.88, 27.86, 21.84, 15.82, and 12.30 dB.

The locations of the X-junctions in the image $\psi_b(x)$ and in each one of its noisy versions $\psi_n(x)$, both referred to as $\psi(x)$ for short henceforth, are first estimated with the corner detector proposed by Harris and Stephens [7], i.e., by computing the function

$$c(x) \doteq \det(M) - 0.04(\text{trace}(M))^2, \qquad (2)$$

with

$$M = \begin{bmatrix} \left(\frac{\partial\psi(x)}{\partial x}\right)^2 \circledast g(x) & \left(\frac{\partial\psi(x)}{\partial x}\frac{\partial\psi(x)}{\partial y}\right) \circledast g(x) \\ \left(\frac{\partial\psi(x)}{\partial x}\frac{\partial\psi(x)}{\partial y}\right) \circledast g(x) & \left(\frac{\partial\psi(x)}{\partial y}\right)^2 \circledast g(x) \end{bmatrix}, \qquad (3)$$

where $g(x)$ is a smoothing operator consisting in a normalized Gaussian filter[4] with standard deviation $\sigma_g = 4$ ($\sigma_g = 8$ for the image of Fig. 4 (g)).

Function $c(x)$ has the property of showing prominent positive peaks in correspondence to corners, such

[3]In the numerical implementation, the filter kernel has size 5×5 pixels.

[4]In the numerical implementation, the smoothing kernel has size 21×21 pixels (51×51 for the image of Fig. 4 (g)).

as T-, X-, and L-junctions; these can therefore be extracted by simple thresholding followed by a convenient morphological shrinking operation [1]. Usually, these estimates are within a couple of pixels from the exact locations of the corners and they can be refined with subpixel accuracy by fitting a quadratic function to a neighborood of each corner location and computing their critical points [1].

We consider only the detection of X-junctions within checkerboard calibration patterns; these can be easily separated from the L-junctions with the following heuristic algorithm. Let $\Omega_{P\times P}^{(k)}$ denote the $P \times P$-pixel neighborhood[5] centered at the k-th junction location estimated from the relative maxima of Eq. (2). The image $\psi(x)$ is first lowpass filtered as $\psi_s(x) \doteq \psi(x)\circledast g(x)$ to remove high frequency contributions due to noise; its digital version is denoted as $\psi_s[n]$, $n \in \mathbb{Z}^2$. Let $\mathcal{A}_N$, $\mathcal{A}_S$, $\mathcal{A}_W$, and $\mathcal{A}_E$ be the areas subtended by $\psi_s[n]$ along the northern, southern, western, and eastern border of $\Omega_{P\times P}^{(k)}$. Let M denote the sum of the two largest of these four numbers and m the sum of the two smallest. If $M > \eta m$, with $\eta = 2$, the k-th junction is declared of type L, of type X otherwise.

For each detected X-junction a quadratic fitting of the intensity profile of the smoothed calibration pattern image is obtained by solving the linear least squares problem [1]

$$\min_{\alpha,\beta,\gamma,\delta,\epsilon,\zeta} \left\|(\alpha x^2 + \beta xy + \gamma y^2 + \delta x + \epsilon y + \zeta) - \psi_s(x,y)\right\|_{\Omega_{2\times2}^{(k)}}^2, \qquad (4)$$

For X-junctions, the quadratic function $z = \alpha x^2 + \beta xy + \gamma y^2 + \delta x + \epsilon y + \zeta$ turns out to be a hyperbolic paraboloid whose critical point, referred to as the saddle point [1], is given by the intersection of the two lines $2\alpha x + \beta y + \delta = 0$ and $\beta x + 2\gamma y + \epsilon = 0$, i.e., $\hat{x}_s^{(k)} =$

[5]In the examples of this paper, we have used $P = 5$ pixels.

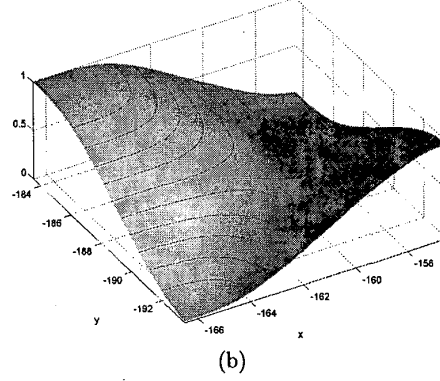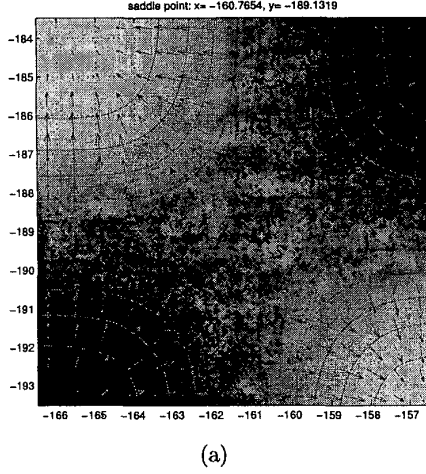saddle point: x= -160.7654, y= -189.1319

(a)

(b)

Figure 2: (a) A detail of the image $\psi_s(x)$ near an X-junction, denoted by a yellow '+.' The solid magenta lines are contour profiles and the arrows denote direction and magnitude of the image gradient. (b) 3-D rendition of the surface $z = \psi_s(x)$ along with contour lines. The saddle point corresponding to the X-junction is marked with a yellow '+.'

$-\left[\begin{smallmatrix} 2\alpha & \beta \\ \beta & 2\gamma \end{smallmatrix}\right]^{-1}\left[\begin{smallmatrix} \delta \\ \epsilon \end{smallmatrix}\right]$; these are the coordinates, computed with subpixel accuracy, of the k-th X-junction. The numerical solution of the problem in Eq. (4) requires a preliminary interpolation of $\psi_s[n]$ over $\Omega_{2\times2}^{(k)}$; in our implementation, we have adopted cubic interpolation.

The histograms of Figs. 3 (b), (e), (h) and 4 (b), (e), (h) show the distributions of the estimation errors $d^{(k)} = \|\hat{x}_s^{(k)} - x_o^{(k)}\|$, where $x_o^{(k)}$ is the true location of the k-th X-junction; the solid red lines are the *Rayleigh probability density functions* (pdf's) approximating the histograms profiles in the least squares sense; their mean values μ_d and standard deviations σ_d are, respectively, reported in the second and third column of Table 1. As expected, the estimation accuracy decreases as the SNR decreases; it should be noticed that, also with very noisy images, like that of Fig. 4 (g), the displacement error has an average of about 0.13 pixels. However, Fig. 4 (h) shows that there might exist outliers greater than half a pixel (the quadratic function in Eq. (4) starts fitting noise too) and this would lead to large errors in the estimation of the intrinsic and extrinsic parameters of the camera [2].

The subpixel refinement can be made computationally simpler and numerically more accurate by observing a close-up of the surface $\psi_s(x)$ (after cubic interpolation) in a neighborhood of a typical X-junction. Fig. 2 (a) depicts one of such neighborhoods and Fig. 2 (b) the 3-D rendition of the associated surface $z = \psi_s(x)$; the X-junction and its corresponding saddle

point are marked with a yellow '+.' The lowpass filter $g(x)$ renders this surface very smooth and makes it easy to determine the location x_s of its saddle point. Mathematically, this point is such that $\nabla\psi = \left[\begin{smallmatrix} \frac{\partial\psi}{\partial x} & \frac{\partial\psi}{\partial y} \end{smallmatrix}\right]^T = 0$, and $\mathcal{H} \doteq \left(\frac{\partial^2\psi}{\partial x^2}\right)\left(\frac{\partial^2\psi}{\partial y^2}\right) - \frac{\partial^2\psi}{\partial x\partial y} < 0$ at $x = x_s$; in terms of numerical computation, this extremal point if found by applying a morphological shrinking operation to the points which meet the two constraints $\|\nabla\psi\| \leq \tau$ and $\mathcal{H} < 0$, where τ is a preselected threshold.

In Figs. 3 (a), (d), (g) and Figs. 4 (a), (d), (g), the X-junctions detected with this simple algorithm are marked with red '+.' The histograms of Figs. 3 (c), (f), (i) and 4 (c), (f), (i) show the distributions of the relative estimation errors $d^{(k)} = \|\hat{x}_s^{(k)} - x_o^{(k)}\|$, where the saddle points $\hat{x}_s^{(k)}$ were estimated with the new algorithm; the solid red lines are the relative Rayleigh pdf's. Their mean values μ_d and standard deviations σ_d are respectively summarized in the fourth and fifth column of Table 1. We may notice that the latter estimates are slightly more precise than the former (they are equal for $SNR = 21.84\ dB$); however they appear to be less sensitive to outliers at high SNR's (compare Figs. 4 (h) and (i)).

3. CONCLUSIONS

This paper has presented a simple method for subpixel detection of X-junctions in images of checker-
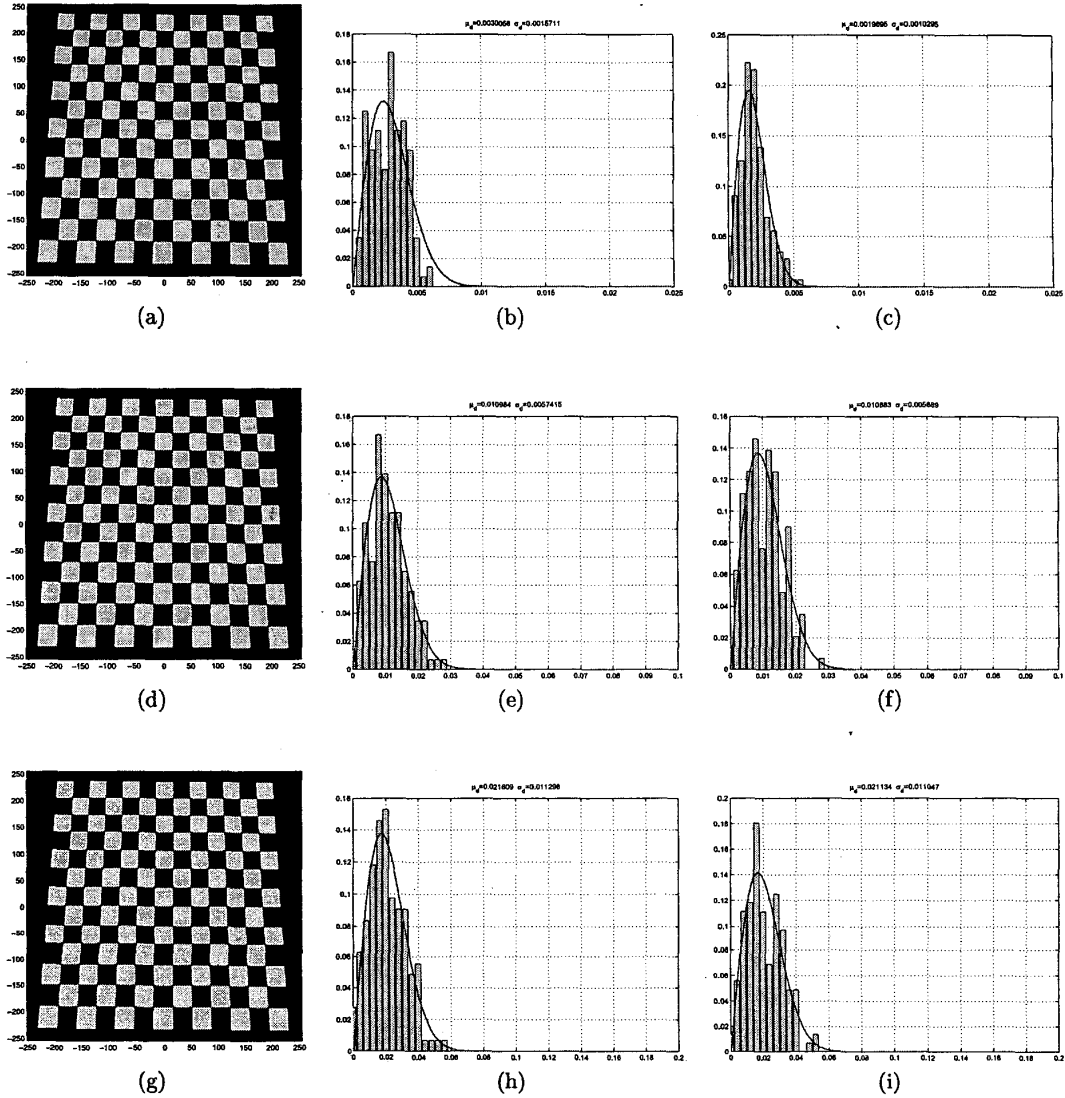
Figure 3: Left column: test images $\psi_b(x)$ (a) and $\psi_n(x)$ with $SNR = 33.88\,dB$ (d) and $SNR = 27.86\,dB$ (g). Central column: distribution of the estimation errors $d^{(k)}$ with traditional subpixel refinement. Right column: distribution of the estimation errors $d^{(k)}$ with proposed subpixel refinement. The solid red lines are the Rayleigh pdf's fitting the histogram profiles in the least squares sense.

boards for camera calibration applications. It is computationally more convenient than standard techniques for subpixel feature detection and yields improved estimates.

REFERENCES

[1] R. Jain, R. Kasturi, and B.G. Schunck, *Machine Vision*, McGraw-Hill, Inc., New York, NY, 1995.

[2] J.-M. Lavest, M. Viala, and M. Dhome, "Do We Really Need an Accurate Calibration Pattern to Achieve a Reliable Camera Calibration?," *Proc. of European Conference on*
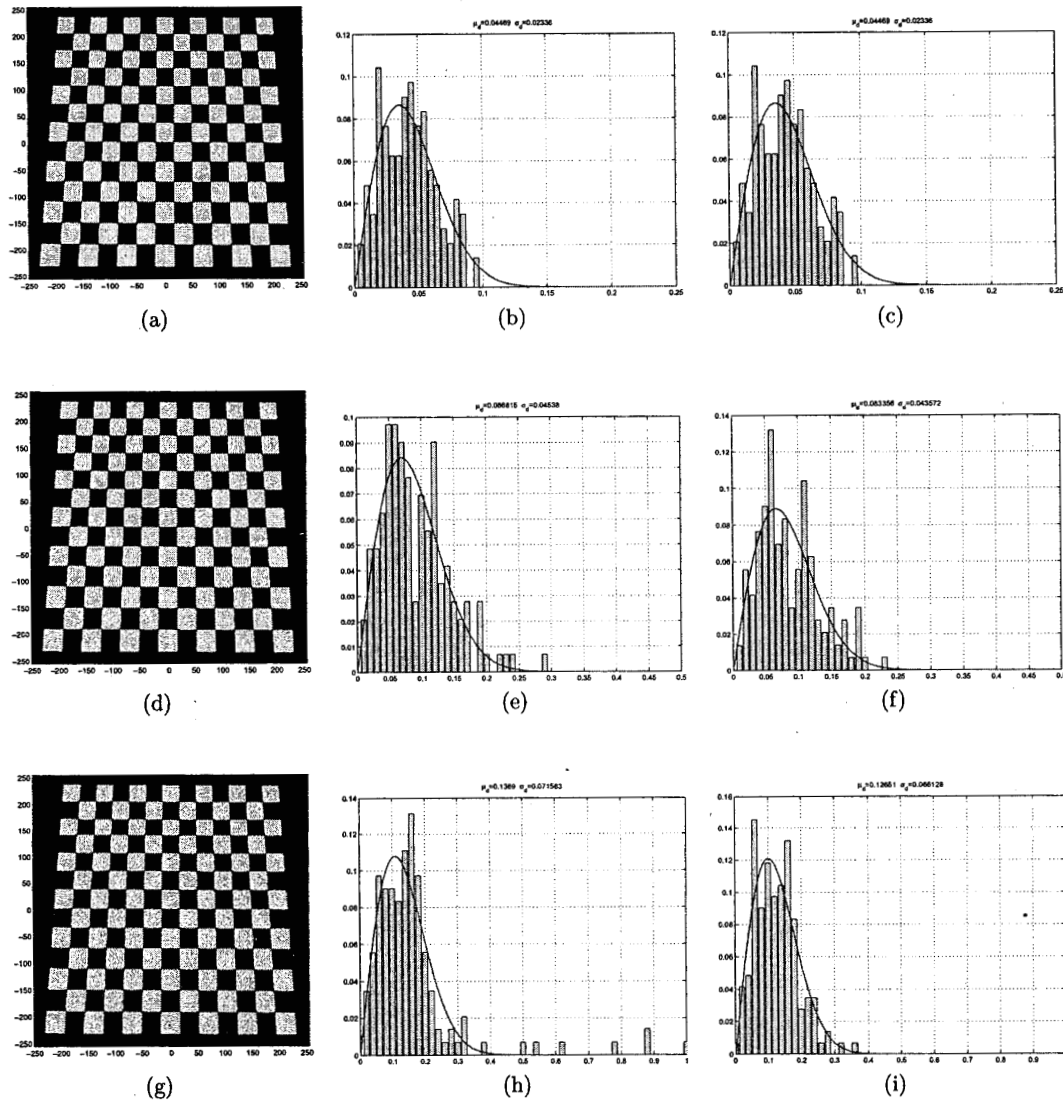
Figure 4: Left column: test images $\psi_n(x)$ with $SNR = 21.84\ dB$ (a), $SNR = 15.82\ dB$ (d), and $SNR = 12.30$ dB (g). Central column: distribution of the estimation errors $d^{(k)}$ with traditional subpixel refinement. Right column: distribution of the estimation errors $d^{(k)}$ with proposed subpixel refinement.

Computer Vision, 1998, Vol. I, pp. 158-174.

[3] J. Heikkilä, "Geometric Camera Calibration Using Circular Points," *IEEE Trans. on PAMI*, Vol. 22, No. 10, pp. 1066-1077, Oct. 2000.

[4] Z. Zhang, "A Flexible New Technique for Camera Calibration," *IEEE Trans. on PAMI*, Vol. 22, No. 11, pp. 13306-1334, Nov. 2000.

[5] B. Peuchot, "Camera Virtual Equivalent Model 0.01 Pixel

Detectors," *Computerized Medical Imaging and Graphics*, Vol. 17, Nos. 4/5, pp. 289-294, 1993.

[6] J.-Y. Bouguet, *Camera Calibration Toolbox for Matlab*, http://www.vision.caltech.edu/bouguet/calib_doc/.

[7] C. Harris and M. Stephens, "A Combined Corner and Edge Detector," *Proc. of the fourth Alvey Vision Conference*, Manchester, UK, Aug. 1988, pp. 147-151.